Role of the interaction processes in the depth-dose distribution of proton beams in liquid water

Rafael Garcia-Molina[1], Isabel Abril[2], Pablo de Vera[2], Ioanna Kyriakou[3] and Dimitris Emfietzoglou[3]

[1] Departamento de Física – Centro de Investigación en Óptica y Nanofísica, Universidad de Murcia, E-30100 Murcia, Spain
[2] Departament de Física Aplicada, Universitat d'Alacant, E-03080 Alacant, Spain
[3] Medical Physics Laboratory, University of Ioannina Medical School, GR-45110 Ioannina, Greece

E-mail: rgm@um.es

Abstract.

We use a simulation code, based on Molecular Dynamics and Monte Carlo, to investigate the depth-dose profile and lateral radial spreading of swift proton beams in liquid water. The stochastic nature of the projectile-target interaction is accounted for in a detailed manner by including in a consistent way fluctuations in both the energy loss due to inelastic collisions and the angular deflection from multiple elastic scattering. Depth-variation of the projectile charge-state as it slows down into the target, due to electron capture and loss processes, is also considered. By selectively switching on/off these stochastic processes in the simulation, we evaluate the contribution of each one of them to the Bragg curve. Our simulations show that the inclusion of the energy-loss straggling sizeably affects the width of the Bragg peak, whose position is mainly determined by the stopping power. The lateral spread of the beam as a function of the depth in the target is also examined.

1. Introduction

The advantages of ion beams in cancer treatment with respect to conventional radiotherapy with photons and electrons are well known [1], due to their characteristic Bragg peak, small lateral spreading and increased relative radiobiological effectiveness (RBE). Nowadays hadrontherapy is a powerful emergent technique used in cancer therapy, especially for deep-seated tumours [2, 3]. Nonetheless, a complete understanding of the relevant involved interactions has not yet been reached, since ion beam radiotherapy involves mechanisms in several spatial and temporal scales [4]. Actually, the whole hadrontherapy problem implies processes from the scale of zeptoseconds and picometers (nuclear fragmentations), passing through femptoseconds and nanometers (primary ion and secondary particles propagation) until millimeters and minutes or even years (tumor death and medical treatments) [5].

In this work we are interested in the first stage of the process, i.e., the depth-dose distribution by the primary ion beam in biological media, since data obtained in this step are needed to model and to understand the subsequent processes. With this aim, we use the Molecular Dynamics and Monte Carlo based code SEICS (Simulation of Energetic Ions and Clusters through Solids) [6] to simulate the motion of fast proton beams in liquid water. Since the code allows us to

Published under licence by IOP Publishing Ltd

follow the trajectory, energy and charge state of each incident projectile through the stopping media, we are able to determine both the spatial evolution of the ion beam and its depth-dose profile. The SEICS code considers inelastic collisions between the projectile and the target electrons, corresponding to the electronic stopping force, where energy-loss fluctuations due to the stochastic nature of these processes are included through the energy-loss straggling. The elastic scattering of the projectile with target atoms is also incorporated in the code, as well as the electron capture and loss mechanism by the projectile. Each of these processes can be switched on and off in the simulation, providing information on their effect in the energy evolution of the primary beam, and in the spatial distribution of energy deposition, that is, into the Bragg curve. Although the energies used in cancer treatment are typically of hundreds of MeV, we will focus on low energies (several MeV), where differences of the order of micrometers in the depth-dose curves are more visible.

The work is structured as follows: section 2 briefly reviews the dielectric formalism to evaluate the stopping power and the energy-loss straggling of fast protons in liquid water, and the MELF-GOS methodology to calculate the electronic excitation spectrum of liquid water. These stopping magnitudes are input quantities into the simulation code SEICS, whose main characteristics are featured in section 3. The results of the simulations are presented in section 4, and the final conclusions are given in section 5.

2. Inelastic energy-loss of swift projectiles

A swift charged particle that is travelling through matter experiences Coulomb interactions with target electrons, resulting in electronic excitations and ionizations. As a consequence, the swift particle transfers energy and momentum to the target, resulting in a slowing down, which depends on its velocity. As the projectile can also lose or capture electrons, it feels a stopping force which is strongly dependent on its charge state.

The dielectric formalism [7, 8] provides the framework to calculate the electronic stopping magnitudes taking into account condensed-phase effects of the irradiated target. For a projectile with atomic number z, mass m, and charge-state q travelling with velocity v through a medium with dielectric function $\epsilon(k,\omega)$, the dielectric formalism states that the statistical moments of the energy loss distribution, $\mathcal{F}_q(n)$, are given by

$$\mathcal{F}_q(n) = \frac{2e^2\hbar^{n-1}}{\pi v^2} \int_0^\infty \frac{\mathrm{d}k}{k} \left[z - \rho_q(k)\right]^2 \int_0^{kv} \mathrm{d}\omega \, (\omega)^n \, \mathrm{Im}\left[\frac{-1}{\epsilon\,(k,\omega)}\right], \tag{1}$$

where $\mathcal{F}_q(1) = S_q$ is the stopping power (mean energy lost per unit path length) and $\mathcal{F}_q(2) = \Omega_q^2$ is the energy-loss straggling (related to the variance of the energy-loss distribution) [9]. Here e is the elemental charge, and $\rho_q(k)$ is the Fourier transform of the projectile electronic density for the charge-state q, which is calculated according to the modified Brandt-Kitagawa model [10, 11]. In this expression, the electronic structure of the target is accounted for by the so-called energy-loss function (ELF), $\mathrm{Im}[-1/\epsilon(k,\omega)]$, which gives the probability of producing an excitation with momentum transfer $\hbar k$ and energy transfer $\hbar\omega$.

Since the electronic stopping magnitudes are strongly affected by the charge-state of the projectile, they must be calculated as a weighted sum over its charge-state fractions

$$\mathcal{F}(n) = \sum_{q=0}^{z} \phi_q \, \mathcal{F}_q(n) \ , \tag{2}$$

with ϕ_q being the probability of finding the projectile with a charge-state q, which depends on the target as well as on the nature and velocity of the projectile. As the dynamical equilibrium is

quickly reached, we use the equilibrium charge fractions from a parameterization to experimental data [12].

The target-dependent magnitude in equation (1) is the ELF. Calculating the excitation spectrum from first principles for condensed phases requires a vast computational effort, and therefore, it is preferable to use semiempirical approaches such as the optical-data models, which are computationaly more feasible and give fairly good results [13, 14]. In these optical-data models, the ELF in the optical limit ($k = 0$) is taken from experimental data and then extended to $k \neq 0$ by suitable dispersion schemes, providing in this manner the whole Bethe surface.

Here the Bethe surface of liquid water is obtained from optical data [15] through the MELF-GOS methodology (Mermin Energy-Loss Function – Generalized Oscillator Strengths). It is based on the separation of the ELF in outer and inner electronic excitation contributions, namely [16, 17],

$$\mathrm{Im}\left[\frac{-1}{\epsilon\left(k,\omega\right)}\right] = \mathrm{Im}\left[\frac{-1}{\epsilon\left(k,\omega\right)}\right]_{\mathrm{outer}} + \mathrm{Im}\left[\frac{-1}{\epsilon\left(k,\omega\right)}\right]_{\mathrm{inner}} . \tag{3}$$

As the inner-shell electrons preserve their atomic character, they can be properly described by their generalized oscillator strengths (GOS) in the hydrogenic approach. Aggregation effects are contained in the outer-electrons excitation contribution to the ELF, which we describe through a weighted sum of Mermin-type ELF. The Mermin dielectric function [18] improved the Lindhard dielectric function for a free electron gas [7], since the damping mechanism of plasmons was introduced phenomenologically, resulting in a more realistic description of the ELF, where the broadening of the excitations is taken into account. Since the Mermin dielectric function has an analytic dependence on the momentum transfer, $\hbar k$, it has the advantage that an extension algorithm to $k \neq 0$ is not necessary, as it is done in other models [14, 19, 20]. A detailed explanation of the MELF-GOS model can be found elsewhere [17].

The most recent set of experimental data for the ELF of liquid water was provided by the Sendai group [15, 21, 22] by using inelastic X-ray scattering spectroscopy (IXSS) to measure the generalized oscillator strength (GOS) of liquid water at several momentum transfers. The IXSS data at the optical limit extend from 6 to 160 eV excitation energies, providing a near complete knowledge of the dielectric response properties of the valence-shells of liquid water. Therefore, we account for the outer electrons contribution to the ELF (at $k = 0$) by fitting the experimental ELF using a sum of Mermin-type ELF, $\mathrm{Im}[-1/\epsilon_{\mathrm{M}}\left(k,\omega\right)]$,

$$\mathrm{Im}\left[\frac{-1}{\epsilon\left(k=0,\omega\right)}\right]_{\mathrm{outer}} = \mathrm{Im}\left[\frac{-1}{\epsilon\left(k\approx 0,\omega\right)}\right]_{\mathrm{exp}} = \sum_i \frac{A_i}{W_i^2}\mathrm{Im}\left[\frac{-1}{\epsilon_{\mathrm{M}}\left(k=0,\omega;W_i,\gamma_i\right)}\right]\Theta(\omega-\omega_{\mathrm{th},i}) \ , \tag{4}$$

where A_i, W_i and γ_i are, respectively, the intensity, position and width of each Mermin-type ELF, and $\omega_{\mathrm{th},i}$ is a threshold energy.

The Bethe surface measurements [21, 22] of liquid water by IXSS at several values of the momentum transfer $\hbar k$ are shown by symbols in figure 1 together with the results of the MELF-GOS model (red solid lines). As can be seen, the Bethe surface obtained by the MELF-GOS method is in very good agreement with experimental data in a wide range of k-values. We want to stress that the choice of the extension algorithm in the ELF is crucial to properly reproduce the Bethe surface. A discussion of the influence of the different methods used to extend the optical ELF of liquid water at non-zero momentum transfer can be found in references [14, 20].

The stopping power and the energy-loss straggling of protons in liquid water have been calculated using the dielectric formalism (equations (1) and (2)) and the MELF-GOS model described previously. The results are shown in figure 2 (black solid lines) as a function of the proton energy and compared with several experimental data for liquid [23, 24, 25] and solid

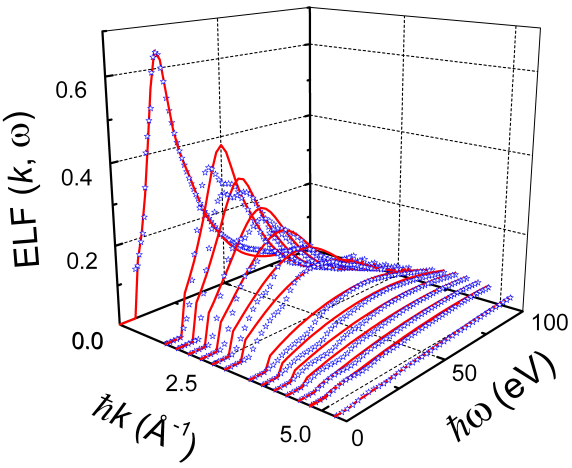

Figure 1. Bethe surface of liquid water. Symbols represent experimental data for several values of the momentum transfer $\hbar k$ measured by the Sendai group [21, 22], whereas solid lines correspond to the MELF-GOS model.

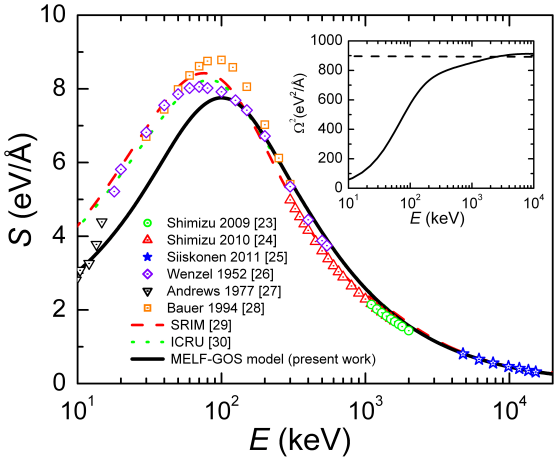

Figure 2. Stopping power S (and energy-loss straggling Ω^2, inset) of liquid water for a proton beam, as a function of its energy. Symbols represent experimental data whereas black solid line corresponds to the MELF-GOS model. See the text for more details.

[26, 27, 28] water (symbols), as well as with semi-empirical calculations such as SRIM [29] (red dashed line) and ICRU recommended data [30] (green dotted line). All the predictions agree quite well at high energies, among them that with the most recent experimental data for liquid water [25], but differences appear at the region of the maximum stopping power. It is worth to note that ICRU and SRIM data are parameterized to ice data, the only ones available at the maximum stopping region. The dielectric calculations with the MELF-GOS model yield lower stopping power values at energies around and below the maximum stopping, which could be attributed to chemical and phase effects, since this model describes self-consistently the electronic excitations of liquid water in a realistic approach, as it has been shown in figure 1.

Stopping power calculations on the depth-dose profile are significant because they mainly determine the most important features of the Bragg curve. Therefore, uncertainties in the stopping power directly produce (undesired) ambiguities in radiotherapy dosimetry. The inset of figure 2 shows the energy-loss straggling of protons in liquid water, as a function of their energy, calculated with the dielectric formalism and the MELF-GOS model. As expected, it tends at high energies to the Bohr straggling limit of a free-electron target, which is depicted by a horizontal dashed line in the figure.

3. Simulation of swift particles moving through liquid water

We have used the SEICS code [6, 31] to simulate the trajectories of fast protons in liquid water, which permits to obtain their spatial and energy distributions at any depth. SEICS is based in Molecular Dynamics and Monte Carlo techniques to follow in detail the motion of a charged projectile through a stopping medium. In each step of the simulation, defined by a time step Δt, the equation of motion of the projectile is numerically solved by the velocity variant of Verlet's algorithm [32] in order to compute its new position $\vec{r}$ and velocity $\vec{v}$

$$\vec{r}(t+\Delta t) \;=\; \vec{r}(t) + \vec{v}(t)\Delta t + \frac{\vec{F}(t)}{2m}\,(\Delta t)^2\,\left[1-(v(t)/c)^2\right]^{3/2}\;, \qquad (5)$$

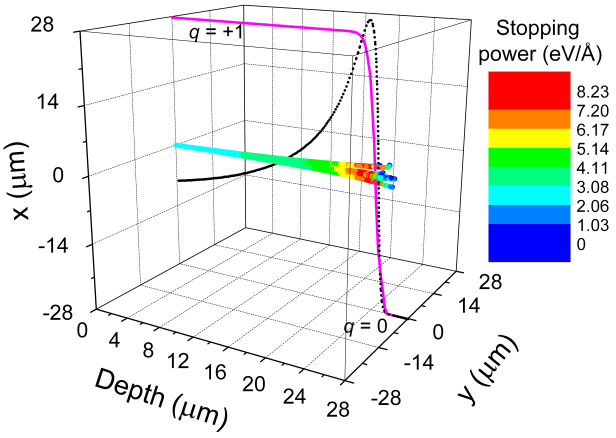

Figure 3. Simulated trajectories corresponding to 1 MeV proton beam incident in liquid water. The graded color along the trajectories represent the stopping power at each depth. The depth-dose curve is shown qualitatively by a dotted black line, and the average charge-state of the projectile by a solid magenta line.

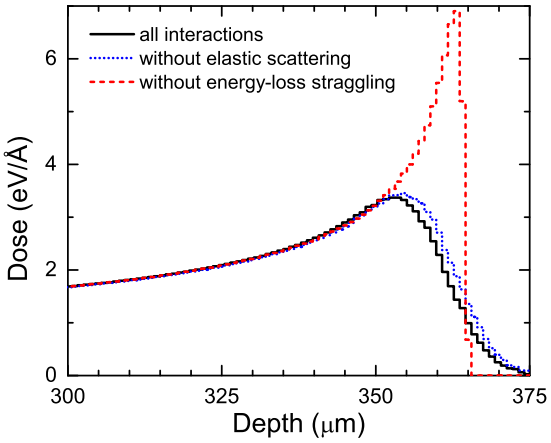

Figure 4. Depth-dose distribution for a 5 MeV proton beam in liquid water. Solid curve represents the result obtained when all the interactions are considered, whereas the dashed and dotted curves where obtained by removing different interactions in the simulation code SEICS.

$$\vec{v}(t+\Delta t) \;=\; \vec{v}(t) + \frac{\vec{F}(t)+\vec{F}(t+\Delta t)}{2m}\,\Delta t\,\left[1-(v(t)/c)^2\right]^{3/2}\;. \tag{6}$$

The factor in brackets is a correction to account for relativistic velocities of the projectiles.

The electronic stopping force $\vec{F}$ that the projectile experiences is obtained from the statistical moments of the energy loss distribution, which were calculated in the previous section with the dielectric formalism and the MELF-GOS model. The stochastic nature of the electronic interactions leads to an electronic stopping force described by a Gaussian distribution centered in the stopping power

$$\vec{F} = -\left[S_q + (\Omega_q/\sqrt{\Delta s})\sqrt{-2\ln\xi_1}\cos\left(2\pi\xi_2\right)\right]\hat{v}\;, \tag{7}$$

where $\hat{v}$ is the unit vector of the instantaneous projectile velocity $\vec{v}$; S_q and Ω_q^2 are, respectively, the stopping power and the energy-loss straggling of liquid water for a projectile with charge q, obtained from equation (1), and $\Delta s = v\Delta t$ is the distance travelled by the projectile in a time step Δt. The symbols ξ_1 and ξ_2 refer to random numbers uniformly distributed between 0 and 1.

To speed up the simulation, at higher projectile energies ($E \geq 10$ MeV/amu) we use the Bohr energy-loss straggling and the Bethe-Bloch stopping power formula [33], with a mean excitation energy $I = 79.4$ eV for liquid water obtained from the MELF-GOS model [31].

The simulation code SEICS also takes into account multiple elastic scattering between the projectile and the target nuclei, by a Monte Carlo algorithm [34, 35] using the universal interatomic potential with a screening length [29]; for more details on the SEICS implementation see reference [6]. Elastic interactions are responsible for the projectile angular deflection and, at the end of their travel, nuclear energy-loss starts to be considerable.

The charge exchange of the projectile due to electron capture and loss processes through the target is also considered in SEICS by a Monte Carlo procedure [6]. In this manner, the charge

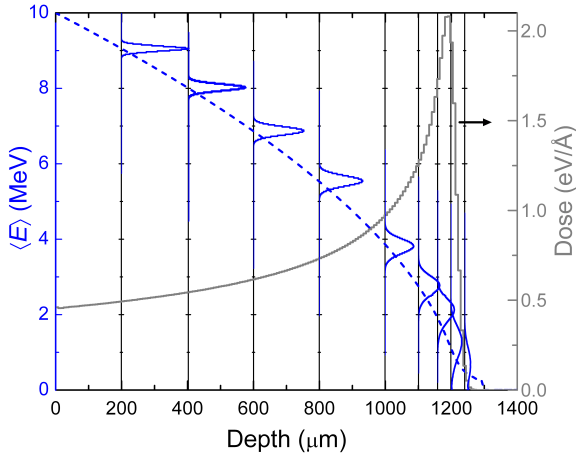

Figure 5. (Left axis) Mean energy (blue dashed line) for a 10 MeV proton-beam incident in liquid water, as a function of its depth. The projectile energy-distributions are depicted by blue solid histograms at several depths. (Right axis) The depth-dose distribution is shown by a grey line.

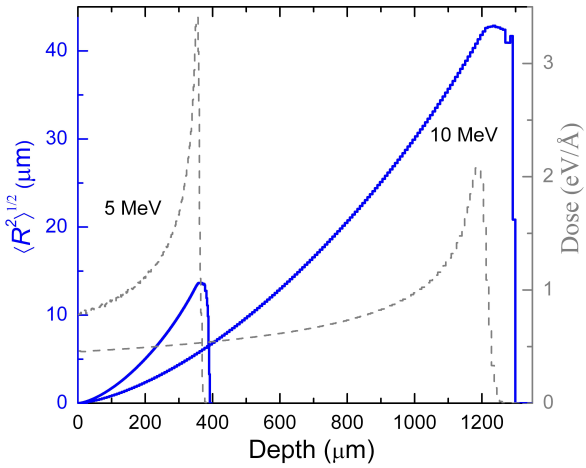

Figure 6. (Left axis) Root mean square radius of the beam (blue solid lines) for 5 MeV and 10 MeV proton beams incident in liquid water, as a function of the depth. (Right axis) The corresponding depth-dose distributions (grey dashed lines) are shown for comparison.

states of the projectile are known along its track, and the stopping power and the energy-loss straggling are calculated at each depth according to the actual charge state of the projectile.

4. Results and discussion

We present the results obtained from the simulation with the SEICS code of the irradiation of liquid water with protons. The main input quantities to be used in the code are the electronic stopping power and the energy-loss straggling, which were obtained in section 2.

Figure 3 depicts several trajectories of 1 MeV protons in liquid water, showing qualitatively the capabilities of the SEICS code, where the graded colors represent the stopping power at each depth. It illustrates (by graded colors) the increase in the dose delivered by the protons along their paths, reaching a narrow maximum at the end of their trajectories (the Bragg peak), where the beam has spread out due to multiple elastic scattering. Although $\sim 10^4$ histories are needed to obtain good statistical results, only a few trajectories are displayed for clarity. The depth dose distribution is depicted by a dotted black line, which clearly represents the Bragg peak. The projectile average charge (magenta solid line) is shown as a function of the depth; note that the mean charge state is +1 in almost all the track, and it rapidly drops to 0 at the end of the Bragg peak. Therefore, at the distal part of the Bragg peak, the number of neutral hydrogen atoms overcomes the number of protons, a fact that is of relevance to determine the secondary electron spectra induced by the primary projectile, which is of most importance to determine the cellular damage at the molecular level.

The simulated depth-dose distribution (i.e. the Bragg curve) of a 5 MeV proton beam in liquid water is shown in figure 4. The black solid line represents the full simulation when elastic scattering and energy-loss straggling are both included in the calculations. By switching on/off the fluctuations in the inelastic energy loss (through the energy-loss straggling) and in the elastic scattering we study how these processes affect the depth-dose profile. The red dashed line represents the depth-dose curve obtained when removing the energy-loss straggling, whereas the

blue dotted line is the simulation without the elastic scattering. As can be seen, both processes practically have no effect on the plateau of the depth-dose curve. Nonetheless, removing the energy-loss straggling does affect the maximum dose region by shifting the Bragg peak to larger depths and strongly narrowing its shape. Removing the elastic scattering has a less important effect, shifting the distal part of the Bragg curve deeper in the target, but not changing its shape. Therefore, the results depicted in figure 4 clearly indicate that the elastic scattering and mainly the energy-loss straggling are essential to determine the right position and shape of the Bragg peak.

The mean energy of the projectile as a function of the depth (blue dashed line) corresponding to a 10 MeV proton beam in liquid water is shown in figure 5. For comparison, the depth-dose curve is shown as a grey solid line. Also, the projectile energy distributions at several depths are depicted by blue (little) histograms, which exhibit a broadening due to the fluctuations in the inelastic collisions accounted for the energy-loss straggling; the reduction of the number of particles as they are stopped is responsible of the smaller size and asymmetry of the deeper histograms. At the Bragg peak the proton beam cannot be considered monoenergetic, so its energy distribution must be carefully taken into account since it is strongly correlated with the spectrum of generated secondary electrons.

Finally, we analyze the lateral spreading of the proton beam in liquid water due to multiple elastic scattering. The root mean square radius of the beam, $\langle R^2 \rangle^{1/2}$, is depicted by solid blue lines in figure 6 for 5 MeV and a 10 MeV proton beams as a function of the depth in liquid water. The corresponding depth-dose curves (grey dashed lines) are also shown for comparison. It is observed how, due to elastic collisions, the mean square radius of the beam increases with the depth following a parabolic dependence, falling off at the distal region of the Bragg curve. This fact is explained by taking into account that only very few projectiles travel in almost a straight line to reach these deep regions. Therefore, as most of the projectiles deviate from their initial direction, they are stopped at lower depths.

5. Conclusions

The depth-dose profile of swift proton beams in liquid water has been simulated by the SEICS code, which is based on Molecular Dynamics and Monte Carlo techniques, allowing a detailed monitoring of the motion of charged particles through condensed media. The simulation includes the following interactions: electronic interaction (evaluated from the stopping power and its fluctuations due to energy-loss straggling), multiple elastic scattering and charge exchange between the projectile and the target due to electron capture and loss processes. A realistic electronic excitation spectrum of liquid water has been used through the MELF-GOS optical-data model, to account for its particular excitation spectrum.

We have evaluated the influence of each interaction in the depth-dose curves of proton beams in liquid water, concluding that fluctuations in the energy-loss processes (through the energy-loss straggling) are fundamental to determine the shape and position of the Bragg peak. Multiple elastic scattering has a minimum effect on the depth-dose distribution, changing the range of the protons only at the distal part of the Bragg curve, nonetheless it is the main responsible of the broadening of the beam profile.

From our results we conclude that, due to the energy-loss straggling, the beam cannot be considered as monoenergetic at the Bragg peak, and that the lateral broadening of the beam increases rather rapidly (with a parabolic dependence) as a function of the depth. These features of the proton beam at the Bragg peak are crucial to describe the spectrum of induced secondary electrons in order to do further and more complex simulations for hadronterapy purposes.

Acknowledgments
This work has been financially supported by the the Spanish Ministerio de Ciencia e Innovación (Project FIS2010-17225) and the European Union FP7 ANTICARB (HEALTH-F2-2008-201587). PdV thanks the Conselleria d'Educació, Formació i Ocupació de la Generalitat Valenciana for its support under the VALi+d program. We acknowledge support provided by the COST Action MP 1002, Nanoscale Insights into Ion Beam Cancer Therapy.

References
[1] Nikjoo H, Uehara S, Emfietzoglou D and Brahme A 2008 *New. J. Phys.* **10** 075006
[2] Kraft G 2000 *Prog. Part. Nucl. Phys.* **45** S473
[3] Goitein M, Lomax A J and Pedroni E 2002 *Phys. Tod.* **55** 45
[4] Solov'yov A V, Surdutovich E, Scifoni E, Mishustin I and Greiner W 2009 *Phys. Rev.* E **79** 011909
[5] Surdutovich E, Scifoni E and Solov'yov A V 2010 *Mutat. Res.* **704** 206
[6] Garcia-Molina R, Abril I, Heredia-Avalos S, Kyriakou I and Emfietzoglou D 2011 *Phys. Med. Biol.* **56** 6475
[7] Lindhard J 1954 *Dan. Vid. Selsk. Mat. Fys. Medd.* **28** No 1
[8] Ritchie R H 1957 *Phys. Rev.* **106** 874
[9] Sigmund P 2006 *Particle Penetration and Radiation Effects. General Aspects and Stopping of Swift Point Charges* (Springer Series in Solid-State Sciences Vol. 151) (Berlin: Springer)
[10] Brandt W and Kitagawa M 1982 *Phys. Rev.* B **25** 5631
[11] Brandt W 1982 *Nucl. Instr. Meth.* **194** 13
[12] Schiwietz G and Grande P L 2001 *Nucl. Instr. Meth.* B **175-177** 125
[13] Ritchie R H and Howie A 1977 *Philos. Mag.* **36** 463
[14] Garcia-Molina R, Abril I, Kyriakou I and Emfietzoglou D 2012 Energy loss of swift protons in liquid water: Role of optical data input and extension algorithms, Ch. 15 in *Radiation Damage in Biomolecular Systems*, eds G García Gómez-Tejedor and M C Fuss (Dordrecht: Springer)
[15] Hayashi H, Watanabe N, Udagawa Y and Kao C C 2000 *Proc. Nat. Acad. Sc. USA* **97** 6264
[16] Abril I, Garcia-Molina R, Denton C D, Pérez-Pérez F J and Arista N R 1998 *Phys. Rev.* A **58** 357
[17] Heredia-Avalos S, Garcia-Molina R, Fernández-Varea J M and Abril I 2005 *Phys. Rev.* A **72** 052902
[18] Mermin N D 1970 *Phys. Rev.* **1** 2362
[19] Emfietzoglou D, Garcia-Molina R, Kyriakou I, Abril I and Nikjoo H 2009 *Phys. Med. Biol.* **54** 3451
[20] Emfietzoglou D, Kyriakou I, Abril I, Garcia-Molina R and Nikjoo H 2012 *Int. J. Radiat. Biol.* **88** 22
[21] Watanabe N, Hayashi H and Udagawa Y 1997 *Bull. Chem. Soc. Jap.* **70** 719
[22] Watanabe N, Hayashi H and Udagawa Y 2000 *J. Phys. Chem. Sol.* **61** 407
[23] Shimizu M, Kaneda M, Hayakawa T, Tsuchida H and Itoh A 2009 *Nucl. Instr. Meth.* B **267** 2667
[24] Shimizu M, Hayakawa T, Kaneda M, Tsuchida H and Itoh A 2010 *Vacuum* **84** 1002
[25] Siiskonen T, Kettunen H, Peräjärvi K, Javanainen A, Rossi M, Trzaska W H, Turunen J and Virtanen A 2011 *Phys. Med. Biol.* **56** 2367
[26] Wenzel W A and Whaling W 1952 *Phys. Rev.* **87** 499
[27] Andrews D A and Newton G 1977 *J. Phys. D: Appl. Phys.* **10** 845
[28] Bauer P, Kaferbock W and Necas V 1993 *Nucl. Instr. Meth.* B **93** 132
[29] Ziegler J F, Biersak J P and Ziegler M D 2008 *SRIM. The Stopping and Range of Ions in Matter* (Chester, MD: SRIM Co). `http://www.srim.org`
[30] International Commission on Radiation Units and Measurements 1993 *Stopping Powers and Ranges for Protons and Alpha Particles* (ICRU Report 49) (Bethesda, MD: ICRU)
[31] Garcia-Molina R, Abril I, Denton C D, Heredia-Avalos S, Kyriakou I and Emfietzoglou D 2009 *Nucl. Instr. Meth.* B **267** 2647
[32] Allen M P and Tildesley D J 1989 *Computer simulation of liquids* (Oxford: Oxford University Press)
[33] Inokuti M 1971 *Rev. Mod. Phys.* **43** 297
[34] Möller W, Pospiech G and Schrieder G 1975 *Nucl. Instr. Meth.* **130** 265
[35] Zajfman D, Both G, Kanter E P and Vager Z 1990 *Phys. Rev.* A **41** 2482